7. Cell line: Methods

7.1. Cell Viability Assay

The inhibition of cell growth by synthesized nanoparticles was assessed by MTT assay [1]. Briefly, cells were seeded in a 96-well cell culture plate in a density of 2500 and 1500 cells/well and left for seeding 24 h prior to test. After completion of 24 h, the old medium was discarded and cells were incubated with various concentrations of pure drug lenalidomide, FePt and SPANS (surface modified pH sensitive Fe_2O_3@FePt alloy nanoconjugates (Fe_2O_3@FePt-NH_2/COOH-Drug-HA-Ctx)) diluted with complete media to yield varying doses (1-50 µg/mL) for a period of 24 and 48 h, respectively. The plates were further incubated at 37 ^{0}C and 5% CO_2 followed by discarding of the samples and washing of the wells with saline. The medium was replaced with serum-free DMEM before the addition of 20 µL of MTT solution (5mg/mL) to each well, and the cells were incubated at 37 °C overnight in the dark. After incubation, 150 µL DMSO was added to the cells after withdrawing the MTT solution to dissolve the MTT Formazan crystals. The plates were then oscillated for 15 min to facilitate the dissolution of Formazan in DMSO. Thereafter, the absorbance was immediately measured at 570 nm by a micro-plate reader (Bio-Rad, Hercules, CA, USA).

7.2. *In vitro* NIR triggered Photothermal, Magnetophotothermal and Chemo-magnetophotothermal Measurement

U87MG cells were seeded in a 24-well plate with a density of 50 000 cells per well [2]. The placebo SPANs were added in wells and incubated with U87MG cells for 4 h. The cells were washed twice with PBS to remove SPANs not taken up by cancer cells, and then fresh PBS (200µL) was added. Cells were then irradiated by 808 nm NIR laser at a power density of 2.5 W cm^{-2} for 5 min. The cell viabilities were determined by a standard MTT assay [1]. For analyzing chemo-photothermal killing of cancer cells, U87MG cells were incubated with drug loaded SPANs (1-50 µg/mL) for 4 hr followed by PBS (200µL) washing to remove free SPANs not taken up by cells. The nanoparticle loaded cells were then irradiated with 808 nm laser (2.5 W cm^{-2}) for 5 min [3]. Cells were then left for 24h and 48h after which the cell viability was determined using standard MTT assay. Pure drug (LND) (1-50 µg/mL) and SPANs (placebo) (1-50 µg/mL) were taken as positive and negative control for SPANs. For assessing chemo-magnetophotothermal killing of cancer cells, U87MG cells were incubated with SPANs (1-50

µg/mL) for 4 hr followed by PBS (200µL) washing to remove free SPANs not taken up by cells. The nanoparticles loaded cells were irradiated with 808 nm laser (2.5 W cm^{-2}) for 5 min by keeping in sample holder employed for inducing magnetic hyperthermia. Cells were the left for 24h and 48h after which the cell viabilities were determined by a standard MTT assay.

7.3. Cell Viability Assay of Surface modified Alloy Nanoparticles

MTT assay was performed to assess cell viability in presence of various surface modified Fe_2O_3@FePt nanoparticles (Fe_2O_3@FePt, Fe_2O_3@FePt-NH_2-HA, Fe_2O_3@FePt-NH_2/COOH, Fe_2O_3@FePt-NH_2-TPPbr, Fe_2O_3@FePt-NH_2-TPP-COOH, Fe_2O_3@FePt-NH_2-TPP-COOH-Ctx, Fe_2O_3@FePt-NH_2/COOH-Drug,Fe_2O_3@FePt-NH_2-TPP-COOH-Drug, Fe_2O_3@FePt-COOH DOTA-NH_2, and Fe2O3@FePt-NH_2-DOTA-NCS). U87MG cells were incubated with various concentrations of surface modified Fe_2O_3@FePt nanoparticles ranging from 1 µg/mL to 50 µg/mL for up to 48 h (24 and 48h), and cell viability was assessed using MTT assay as discussed above.

7.4. *In vitro* BBB Passage/Flux Study

In vitro BBB model was used for assessing the flux of LND, Fe_2O_3@FePt and SPANs on across the BBB. An *in vitro* BBB co-culture model and monolayer model was utilized to investigate the permeation. *In vitro* BBB model was adopted from previously reported literature [4]. The monolayer model was developed using single cell line while co-culture model was developed using two cell lines culture together. In the co-culture model, U-373 MG cells were seeded onto the apical side of inserts (Corning, NY, coated with 2% (w/v) gelatin solution) at a density of 7.5-10^4 cells/well and were allowed to grow for 30 min. The inserts were then transferred to 12-well culture plates containing 1 ml of DMEM medium and were incubated at 37 ^{0}C for 24 h. After incubation, MDCKII cells were seeded onto the inner side of the insert at a density of 150-10^4 cells/well and incubated at 37 ^{o}C for 24 h. After incubation, LND, FePt, Fe_2O_3@FePt and SPANs were diluted with serum-free DMEM which was then applied to the luminal chamber of inserts at concentrations of 1000µl per well (2 mg/mL). After treatment with samples, 200µl of medium was withdrawn from basal chamber at 0, 2, 24 and 48 h and the medium was replenished with 200µl of fresh serum-free DMEM to maintain the sink condition. The permeation of drug through the *in vitro* BBB model was determined through fluorescence

spectroscopy (FSX100 (Olympus, USA)) and the transport ratio of lenalidomide, while ICP-OES was used for determining Fe_2O_3@FePt and SPANs across the *in vitro* BBB model and was calculated using the formula given below:

$$Transport\ ratio\ (\%) = \left(\frac{Wn}{W}\right) * 100$$

Where, Wn=amount of lenalidomide in basal chamber at time "n" (n=2, 24 and 48 h); W= amount of lenalidomide added in apical chamber.

For estimation of Fe_2O_3@FePt; Wn=amount of Fe_2O_3@FePt in basal chamber at time "n" (n=2, 24, 48); W=amount of Fe_2O_3@FePt added in apical chamber. Similar calculation was done for SPANs.

For *in vitro* permeation of LND, Fe_2O_3@FePt and SPANs using the monolayer model, the cells were grown in a fashion similar to the co-culture model but only one cell line (MDCKII) was used and the formulations were subjected to monolayer cell line model study.

The *in vitro* BBB passage study was also performed in presence of alternating magnetic field (AMF) to assess effect of hyperthermia on permeation of nanoparticles through BBB.

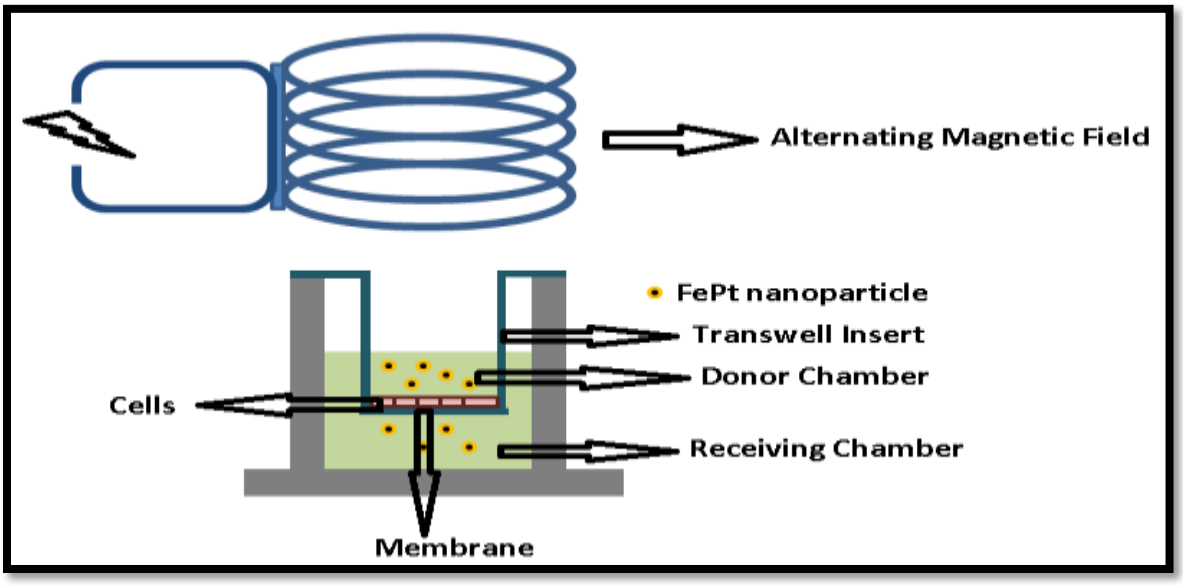

Figure 7.1: Outline for carrying out *In vitro* BBB passage study with and without AMF.

Cells were incubated with LND, Fe_2O_3@FePt and SPANs (1-50 µg/mL) for 4 hr followed by PBS (200µL) washing to remove free SPANs not taken up by cells. The inserts were then kept in

sample holder employed for inducing magnetic hyperthermia for 5 minutes with applied frequency of 265 kHz as depicted in Figure 7.1. A control study was also performed without AMF

7.5. Estimation of ROS Generation

For determination of ROS, U87MG cells were seeded in 96 well plate for 24 h followed by treatment of LND (1-50 µg/mL), Fe_2O_3@FePt (1-50 µg/mL) and SPANs (1-50 µg/mL) together with 10 µg mL^{-1} of H_2O_2. ROS was determined by addition of dye H_2DCFDA (2,7-dichlorodihydrofluorescein diacetate) to LND, Fe_2O_3@FePt and SPANs treated cells. The dichlorofluorescein (DCF) fluorescence was recorded at 535 nm. This was repeated in triplicate independently. The background fluorescence was subtracted to calculate fluorescence of DCF using plate reader (Fluoroskan Ascent CF (Labsystems, USA)). The generated ROS was expressed as a ratio of the fluorescence of DCF of treated cells to that of untreated cells.

For analyzing the effect of magnetic field on ROS generation by LND, Fe_2O_3@FePt and SPANs, amount of ROS generated from the surface of LND, Fe_2O_3@FePt and SPANs was estimated using methylene blue degradation assay according to previously described method with slight modification [5]. Working samples were prepared by diluting stock concentrations of methylene blue to 5 µg/mL and LND, Fe_2O_3@FePt and SPANs to75 µg/mL. The samples were placed in the water bath maintained at 37^oC for 10 min to equilibrate to the expected steady state temperature as a result of magnetic field exposure. The degradation was induced by spiking 30% H_2O_2 to the samples with a working concentration of 245 mM. The samples were exposed to a magnetic field approximately 51.0 kA/m in strength at 292 kHz frequency by keeping it in centre of the coil with applied frequency of 292 kHz. After given time intervals (5 min and 10 min) the samples were magnetically decanted using NdFeB permanent magnet, and degradation of methylene blue was determined using UV–visible spectroscopy (maximum absorbance at 665 nm) with a UV 1800 (Shimadzu, Japan). To account for nanoparticles scattering from the nanoparticles that remain in suspension, samples containing only nanoparticles were measured and subtracted out from the sample absorbance.

7.6. Colony forming assay

The CFA or colonogenic assay is a classical test to evaluate cell growth and assess the functional integrity of cells after treatment. The regeneration potential of cancer cell lines after treatment with radiation or anticancer agents and cellular morphology can also be investigated with this method. To test cell proliferation or regeneration potential, cell lines are treated with anticancer agents in multiwell plates. After the incubation period, cells are fixed, stained and number of colonies defined as group of neighboring cells that are thought to be oriented from mother cells are to be counted. Regeneration potential of U-87 MG cells in presence of anticancer formulations were determined by using colony formation assay. Colonogenic assay was carried out to assess the long term cytotoxicity of different formulations. 600 U87MG cells were seeded in a 35 mm plate and after stabilization [6] treated with FePt, SPANs and Fe_2O_3@FePt nanoparticles at a concentration of 25µg/mL (1 mL). These were removed after an incubation period of 24 h, and the plates were washed with PBS to remove traces of the drug. Cells were later incubated in DMEM for a period of 8–10 days. Cells were fixed using 70% chilled methanol followed by staining using 1% Crystal violet. Colonies containing 50 or more cells were counted.

7.7.Estimation of Intracellular uptake

The uptake of SPANs (Fe_2O_3@FePt-NH_2/COOH-Drug-HA-Ctx) and Fe_2O_3@FePt nanoparticles was investigated using particles loaded with FITC, a hydrophilic dye. Sub-confluent cultures of U87MG cells were treated with only FITC and FITC conjugated SPANs for 2 h respectively. Cells were later washed with PBS and fixed using 1% paraformaldehyde (PFA). The cells were then treated with DAPI and then washed thrice with PBS. Coverslips were mounted using 2.5% DABCO on glass slides and then sealed with nail paint. Images were acquired on LSM 510 confocal microscope from Zeiss at 63X. LSM image browser software was used for data analysis. The subconfluent cultures of U-87MG cells ($5x10^3$) grown on coverslips (37^0 C, 24h) were treated with FITC labeled SPANs (0.8mg/mL and 1.2 mg/mL) for 12h. Cells were washed with PBS and fixed using 1% PFA. The coverslips were mounted using 2.5% (DABCO) on glass slides and sealed. The acquisition was done using Zeiss LSM 510 confocal microscope (Germany) at 60x (excitation wavelength=488 nm, emission wavelength=560 nm). Prussian blue staining was also done to visualize internalization of SPANs in U-87MG cells. Briefly, cells

were fixed in methanol (at −20°C) for 5 min, stained with an equal volume of 4% hydrochloric acid and 4% potassium ferrocyanide for 15 min, and counterstained with 0.5% neutral red for 2 min. The cells were then visualized under microscope (FSX100 (Olympus, USA)). Quantitative estimation of iron was also performed using ICP-OES (Perkin Elmer Optima 5300 DV).

7.8. Cellular Uptake Mechanism Study

In order to understand endocytosis mechanism of SPAN (Fe_2O_3@FePt-NH_2/COOH-Drug-HA-Ctx) and M-SPANs (Fe_2O_3@FePt-NH_2/COOH-TPP-Drug-HA-Ctx), cellular uptake mechanism study was done by using different inhibitors that are known to block different uptake pathways [7]. U87MG cells were seeded in 6 well plates at a density of $2x10^5$cells/mL and incubated for 48h. After 30 min incubation in DMEM, the cells were treated with 200µg/mL of SPANs, M-SPANs and inhibitors (PBS (control), chlorpromazine (50µM) for inhibiting clathrin based endocytosis; amiloride (50µM) for inhibiting macropinocytosis; genistein (200µM) for inhibiting caveolae based endocytosis) for 1h respectively. After washing with ice cold PBS and acid buffer at 4^oC, the cells were removed from the wells by using trypsin, digested with Nitric acid and estimation was done using ferrozine iron assay.

7.8.1. Ferrozine Iron Assay

Uptake of iron nanoparticles by cells were quantitatively assessed by ferrozine iron assay. The nanoparticles incubated U87MG cells in 24 wells were frozen at −20°C for 1 h followed by addition of 500 µl of 50 nM NaOH each well and left undisturbed for 2 h. Aliquots of cell lysates were then transferred to 1.5 ml eppendorf and mixed with 500 µl of 10 mM HCl along with 500 µl of iron-releasing reagent (a freshly mixed solution of equal volumes of 1.4 M HCl and 4.5% (w/v) $KMnO_4$ in distilled H_2O) and left at 70 C for 1 h. After the temperature of mixtures cooled to room temperature, 150 µl of iron-detection reagent (6.5 mM ferrozine, 6.5 mM neocuproine, 2.5 M ammonium acetate, and 1 M ascorbic acid dissolved in water) were added to each tube. After 30 min incubation, After 30 min, the solution in each tube was transferred into a well of a 96 well plate and absorbance measured at 550 nm on a micro-plate reader. A standard curve was prepared with 0, 0.1, 0.2, 0.5, 1, 2, 5, and 10 µg/mL iron ($FeCl_3$), and similarly treated [8].

7.9. Mitochondrial Localization

U-87MG cells were cultured in 24 well plates for 24h. The cell media were replaced with FITC labeled SPANs (Fe_2O_3@FePt-NH_2/COOH-Drug-HA-Ctx) and M-SPANs (Fe_2O_3@FePt-NH_2/COOH-TPP-Drug-HA-Ctx) dispersion (200µL, 25µg/mL) in U87MG culture medium and allowed to incubate for 12h. The labeled nanoparticles were excited at 488 nm and emission wavelength was collected at 560 nm using Zeiss LSM 510 confocal microscope (Germany) at 60X. The mitochondrial localization of both SPANs and M-SPANs was analyzed by overlaying fluorescent images of red and green channels.

7.10. Fluorescence Analysis of Isolated Mitochondria

To assess and further confirm the targeted delivery of SPANs (Fe_2O_3@FePt-NH_2/COOH-Drug-HA-Ctx) and M-SPANs (Fe_2O_3@FePt-NH_2/COOH-TPP-Drug-HA-Ctx) into mitochondria, fluorescence analysis of isolated mitochondria was conducted based on molecular fluorescent characters of FITC labeled SPANs and M-SPANs. The U87MG cells were incubated with FITC labeled SPANs and M-SPANs (200µL, 25µg/mL) for 24h. The isolation of mitochondria from U87MG cells was performed by using a mitochondria isolation kit for cultured cells (Thermo Scientific, USA). U87MG cells were cultured in culture flask at a density of 1×10^7. The cells were harvested with trypsin treatment. Mitochondria were isolated from the cells as per published protocol (Briefly, U87MG cells were grown until confluent, washed in phosphate-buffered saline. Cells ($\sim 2 \times 10^8$) were pelleted at 500 × *g* for 5 min at room temperature and resuspended in 30 ml of isolation buffer (220 mM mannitol, 70 mM sucrose, 1 mM EDTA, 0.5 mM PMSF, 2 mg/ml bovine serum albumin, 20 mM Hepes-KOH, pH 7.4) before mitochondrial isolation. The pellet was dispersed in 40 ml of isolation buffer (without bovine serum albumin) and centrifuged at 1800 rpm for 10 min. The upper three-quarters of the supernatant was removed and further centrifuged at 7000 rpm for 10 min. The resulting pellet was uniformly suspended in 10 ml of isolation buffer (without bovine serum albumin) and centrifuged at 1800 rpm for 10 min. The supernatant was centrifuged at 7000 rpm to collect purified mitochondria. They were suspended in a medium containing 10 mM Hepes, pH 7.4, 0.25 M sucrose, 1 mM dithiothreitol, 10 m~ Na succinate, 0.15 mM ADP, and 2.5 mM K_2HPO_4, pH 7.4. Mitochondria were stored in 0.5 mg/ml aliquots in storage buffer (500 mM sucrose, 10 mM Hepes-KOH, pH 7.4) at −80 °C prior to use) [9]. After that, mitochondria containing pellet was suspended in PBS

(200 µL) and then the PBS was transferred to 96-well plate. The fluorescence intensity at excitation wavelength of 488 nm was measured by using micro-plate reader (Fluoroskan Ascent CF (Labsystems, USA)).

7.11. Detection of Changes in Mitochondrial Membrane Potential

Qualitative changes in $\Delta\Psi m$ were determined as the changes in tetramethylrhodamine methyl ester (TMRE) fluorescence in quench mode in U87MG cells. Cells were allowed to grow and reach approximately 80% confluency after which they were washed with PBS and detached using trypsin. The cell suspension was centrifuged at 500xg for 5 min. The obtained pellet was resuspended in DMEM containing 50 nM TMRM for 20 min with gentle shaking. The cells suspension was centrifuged and pellet was suspended in warm DMEM containing SPANs (Fe_2O_3@FePt-NH_2/COOH-Drug-HA-Ctx) (25µg/mL, 200µL) and M-SPANs (Fe_2O_3@FePt-NH_2/COOH-TPP-Drug-HA-Ctx) (25µg/mL, 200µL) for 30 min. A FACSCalibur flow cytometer (BD Biosciences, USA) was used to read fluorescence with an excitation wavelength of 488 nm.

7.12. Intracellular ATP Level Detection

The changes in intracellular ATP level detection was performed using ATP determination kit (Invitrogen) using measuring procedures as per the manufacturer's protocol. U87MG cells were seeded in a 6-well plate at cell density of 1×10^5 per well. After incubating cells for 24 h, old medium was removed and new medium (DMEM, 2.0 mL per well) containing SPANs (Fe_2O_3@FePt-NH_2/COOH-Drug-HA-Ctx) and M-SPANs Fe_2O_3@FePt-NH_2/COOH-TPP-Drug-HA-Ctx) (25µg/mL, 200µL) were added. After another 24 h of incubation, cells were washed with PBS (2 mL) twice and then treated with cell lysis buffer (200 µL). Cell debris was collected as ATP containing experimental sample. ATP levels were analyzed using Luminescent ATP Detection Assay Kit (Invitrogen, USA) according to the manufacturer's instructions. ATP concentration was calculated by plotting standard curve.

7.13. Analysis of Respiratory Chain Enzymatic activity

Effect of SPANs (Fe_2O_3@FePt-NH_2/COOH-Drug-HA-Ctx) and M-SPANs (Fe_2O_3@FePt-NH_2/COOH-TPP-Drug-HA-Ctx) on enzymatic activity of individual mitochondrial respiratory chain complexes was measured in U87MG cells. Effect of SPANs and M-SPANs on

mitochondrial respiratory chain activity was analyzed according to previously published literature with slight modification [10]. Cell homogenate was prepared and exposed to rapid freeze thaw cycles before using it to measure activity of mitochondrial respiratory chain complex I, II, III and IV.

Complex I assay was assessed in assay mixture containing 25 mM potassium phosphate, 3.5g/l BSA, 2 mM ethylenediaminetetracetic acid (EDTA), 60 µM DCIP (2,6-dichloroindophenol), 70 µM decylubiquinone, 1 µM antimycin A and 0.2 nM reduced nicotinamide adenine dinucleotide NADH, pH 7.8. Rotenone sensitivity was calculated by subtracting activity of well using 10µM rotenone at 600 nm. For complex II activity, assay mixture containing 80 mM potassium phosphate, 1 g/l BSA, 2 mM EDTA, 80 µM DCIP, 10 mM succinate, 50 µM decylubiquinone, 1 µM antimycin A and 3 µM rotenone, pH 7.8. Absorbance was calculated at 600 nm. Maloanate sensitivity activity was calculated by subtracting the activity of wells with 20 mM malonate. Complex III was assessed using assay mixture containing 50 µM ferricytochrome C, 25 mM potassium phosphate, 4 mM sodium azide, 0.1 mM EDTA, 0.025% Tween 20 and 50 µM decylubiquinol, pH 7.4. Antimycin A sensitivity was calculated by subtracting activity of wells using 10 µM antimycin A by measuring absorbance at 550 nm. Complex IV activity was analyzed using assay mixture containing 30 mM potassium phosphate and 25 µM of freshly prepared ferricytochrome C, pH 7.4. The absorbance was calculated at 550 nm.

7.14. RESULTS AND DISCUSSION

7.14.1. Cell lines and Culture Conditions

The cells U87MG and 373MG cells were obtained from the cell respiratory facility of National Center of Cell Sciences, Pune, India. The cell lines were maintained at 16h prior to the experiments as monolayer cultures in Dulbecco's modified Eagle culture medium (DMEM) supplemented with 10% heat inactivated fetal calf serum (FCS) and 1% antibiotic (streptomycin + penicillin). Cultures were maintained at 37˚C in a humidified 5% CO_2 atmosphere. Madin–Darby canine kidney cells (MDCKII, NCCS, Pune, India) were cultured in MEM with 5% FBS and 100 mg/ml streptomycin at 37°C in a humidified incubator with 5% CO_2. The protocols for freezing the cells from existing stock, starting the cell culture from frozen stock, expanding the cell culture and counting the cells are based on the protocols and methodology described in Culture of Animal Cells: A Manual of Basic Technique and Specialized Applications, Sixth Edition, Ed: Freshney R. I., Wiley- Blackwell Publication, 2010.

7.15. Cell Viability Assay

The cellular toxicity of FePt nanoparticles, LND and SPANs (surface modified pH sensitive Fe_2O_3@FePt alloy nanoconjugates (Fe_2O_3@FePt-NH_2/COOH-Drug-HA-Ctx)) were evaluated using U87MG cells. U87MG cells were incubated with various concentrations of FePt nanoparticles, LND and SPANs ranging from 1 µg/mL to 50 µg/mL for up to 48 h (24 and 48h), and cell viability was assessed using MTT assay (Figure 7.2 and 7.3). The cell viability at 1 µg/mL FePt nanoparticles after incubation for 24h was almost 100% while after 48 h it decreased to 97.2%±3.7%. With increase in concentration of FePt concentration, cell viability decreased linearly.

A maximum 69.3%±3.2% cell viability was observed at highest concentration (50µg/mL). In case of LND, 48.5%±2.4% cell viability was observed at concentration of 25µg/mL after 24 h and 41.7%±2.9% after 48h. In case of SPANs, 54.3%±3.7% cell viability was observed at dose concentration of 10µg/mL after incubation for 48h which was much lower than that observed for FePt nanoparticles (82.5%±3.1%) and LND (61.7%±3.5%) at same concentration. At highest concentration of 50µg/mL, only 32.2%±4.1% and 27.5%±3.2% cell viability was observed after 24h and 48h respectively. The enhanced suppression of cell viability in case of SPANs can be attributed to the synergistic activity of FePt and LND. The calculated p-

value for LND with respect to FePt was 0.005, while for SPANs it was 0.003. Similarly, p-value for SPANs with respect to LND and FePt was 0.03 and 0.04 respectively which confirms that the obtained difference in the results of cell viability was due to significant difference in activity of each sample. The increase in suppression of cell viability for SPANs as compared to LND can

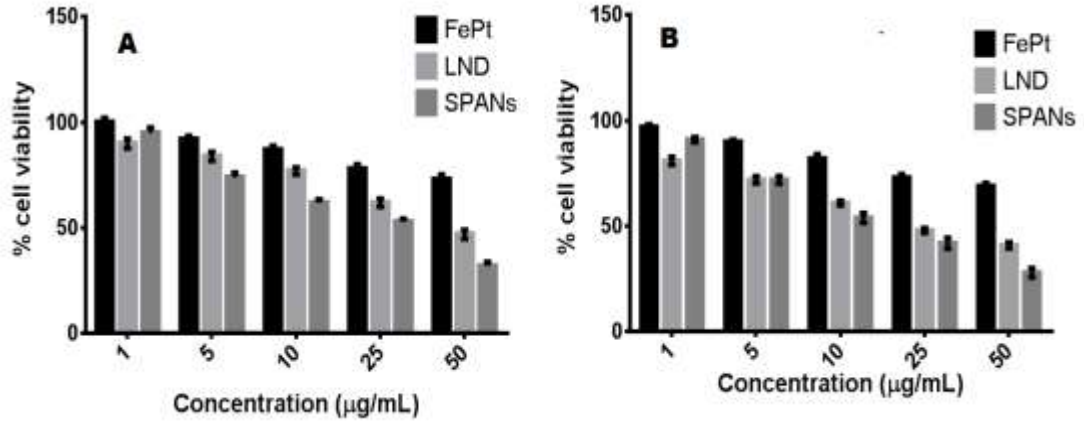

Figure 7.2: *In vitro* cell viability study in U87MG cells using FePt, LND and SPANs after 24 h (A) and 48 h (B).

also be correlated to the fact that incubation for more than 24 h caused internalization of SPANs in nucleus where LND after being released decrease the expression of angiogenic factor VEGF and Interleukin-6 [12]. It also alters VEGF levels, inhibits phosphorylation of Akt and Gab 1 protein. These activities of LND lead to enhanced suppression of cell viability of U87MG. Internalization of SPANs in nucleus after 24h results increased concentration of Fe and Pt inside nucleus which interfere cellular metabolism and intercalation with DNA respectively [13]. Such interaction of Fe and Pt inside nucleus in addition of activities of LND combined helps in enhanced suppression of U87MG cell viability.

7.16. *In vitro* NIR triggered Photothermal, Magnetophotothermal and Chemo-magnetophotothermal Measurement

Various therapies have been explored in animal model for developing an efficient therapy for treatment of cancer. There have been reports regarding use of plasmonic nanoparticles which caused heating upon optical excitation but their biopersistence posed a limitation [14]. In contrast to other nanoparticles, iron nanoparticles are biodegradable and have advantage over other metallic nanoparticles and hence have been explored for photothermal therapy. Apart from photothermal heating ability, iron nanoparticles possess the ability for generating magnetic

hyperthermia having unlimited tissue penetration but it involves larger dose of nanoparticles to achieve temperature rise enough for tumor therapy [15].

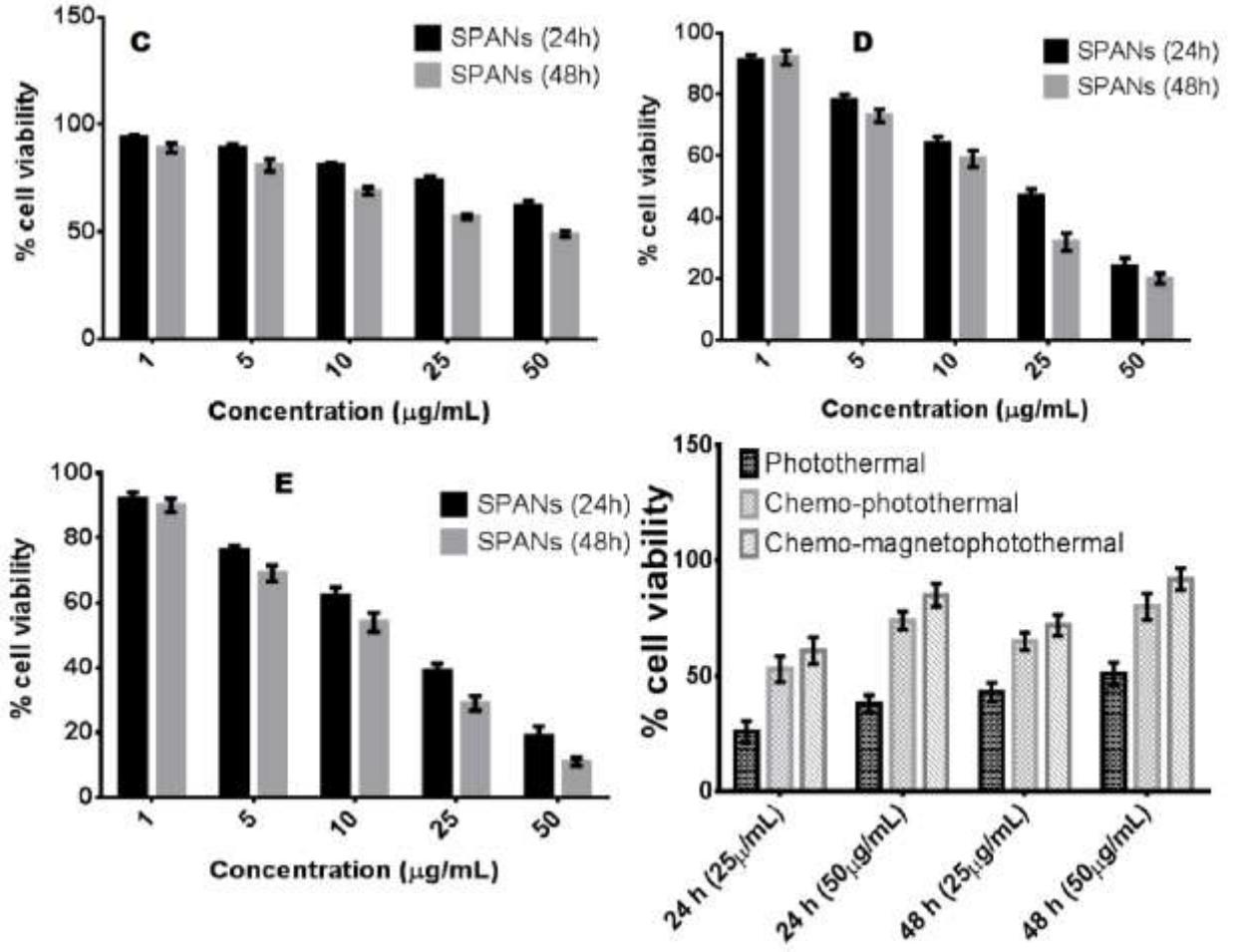

Figure 7.3: Photothermal killing using SPANs (placebo) (C), chemo-photothermal killing using SPANs (D), chemo-magnetophotothermal killing using SPANs (E). Comparative cell viability has been shown for multimodal killing of U87MG cells (F).

Keeping in mind the abovementioned facts, an attempt was made to develop a system having multimodal therapeutic ability which includes chemothermal ability, photothermal ability and magnetothermal ability. Figure 7.3 (A, B, C) represents the comparative in vitro cell killing ability of developed system. In photothermal therapy, placebo SPANs were used for studying suppression of cell viability in U87MG cells. Although no significant decrease in cell viability was observed at dose of 5μg/mL and 10μg/mL, a 38.3%±4.1% and 51.7%±3.9% decrease in cell viability was observed at the highest studies dose of 50μg/mL after 24h and 48h respectively. An

enhancement in suppression of cell viability was observed in case of chemo-photothermal killing of cancer cells owing to cell killing ability of LND. The decrease in cell viability observed (53.5%±3.8% and 65.4%±5.7% after 24h and 48h respectively at dose of 25µg/mL) was at half the dose of that required in case of photothermal therapy. The reason for enhanced efficacy of chemo-photothermal therapy over chemotherapy can also be attributed to the fact that photothermal effect of FePt nanoparticles causes formation of characteristic cavities in cells along with loss of cellular membrane integrity which helped increase in cellular uptake of nanoparticles and ultimately drug causing decrease in cell viability [16]. In case of chemo-magnetophotothermal therapy the decrease in cell viability was unprecedented and was much better than photothermal therapy alone or in combination with chemotherapy. The decrease in cell viability was 61.3.%±4.5% and 72.6%±5.3% after 24h and 48h respectively at dose of 25µg/mL. The enhanced suppression of cell viability can be attributed to the synergistic activity of heat generation by photothermia, magnetic hyperthermia and chemotherapy. The enhanced decrease in cell viability after 48 h is due to increase in cellular uptake as well as nuclear localization of SPANs in comparison to 24h.

7.17. Cell Viability Assay of Surface modified Alloy Nanoparticles

MTT assay was performed to assess cell viability in presence of surface various surface modified Fe_2O_3@FePt nanoparticles (Fe_2O_3@FePt, Fe_2O_3@FePt-NH_2-HA, Fe_2O_3@FePt-NH_2/COOH, Fe_2O_3@FePt-NH_2-TPPbr, Fe_2O_3@FePt-NH_2-TPP-COOH, Fe_2O_3@FePt-NH_2-TPP-COOH-Ctx, Fe_2O_3@FePt-NH_2/COOH-Drug,Fe_2O_3@FePt-NH_2-TPP-COOH-Drug, Fe_2O_3@FePt-COOH-DOTA-NH_2, and Fe2O3@FePt-NH_2-DOTA-NCS). U87MG cells were incubated with various concentrations of surface modified Fe_2O_3@FePt nanoparticles ranging from 1 µg/mL to 50 µg/mL for up to 48 h (24 and 48h), and cell viability was assessed using MTT assay. The result of same is shown is figure 7.4. Except for drug conjugated nanoparticles, none of the nanoparticles demonstrated more than 50% suppression of cell viability. Fe_2O_3@FePt-NH_2/COOH-Drug,Fe_2O_3@FePt-NH_2-TPP-COOH-Drug demonstrated 35.8%±2.6 and 32.6%±3.1% cell viability at 50µg/mL concentration. Fe_2O_3@FePt-NH_2-TPP-COOH, Fe_2O_3@FePt-NH_2-TPP-COOH-Ctx demonstrated 68.1%±2.9 and 64.7%±3.2% cell viability at similar concentration. Fe_2O_3@FePt (72.7%±3.1%), Fe_2O_3@FePt-NH_2-HA (75.9%±2.2%), Fe_2O_3@FePt-NH_2/COOH, Fe_2O_3@FePt-NH_2-TPPbr (71.3%±3.5%, Fe_2O_3@FePt-COOH-

DOTA-NH_2 (72.1%±2.9%), and Fe2O3@FePt-NH_2-DOTA-NCS (71.4%±3.3%) showed less than 75% cell viability at 50µg/mL concentration demonstrating that these surface modifications contributes very little to cell killing ability of Fe_2O_3@FePt nanoparticles. Meanwhile, conjugation of TPP to Fe_2O_3@FePt nanoparticles did enhance the cell killing ability of Fe_2O_3@FePt nanoparticles which can be correlated to the fact that conjugation of TPP helps localization of nanoparticles inside mitochondria leading to enhanced cell death.

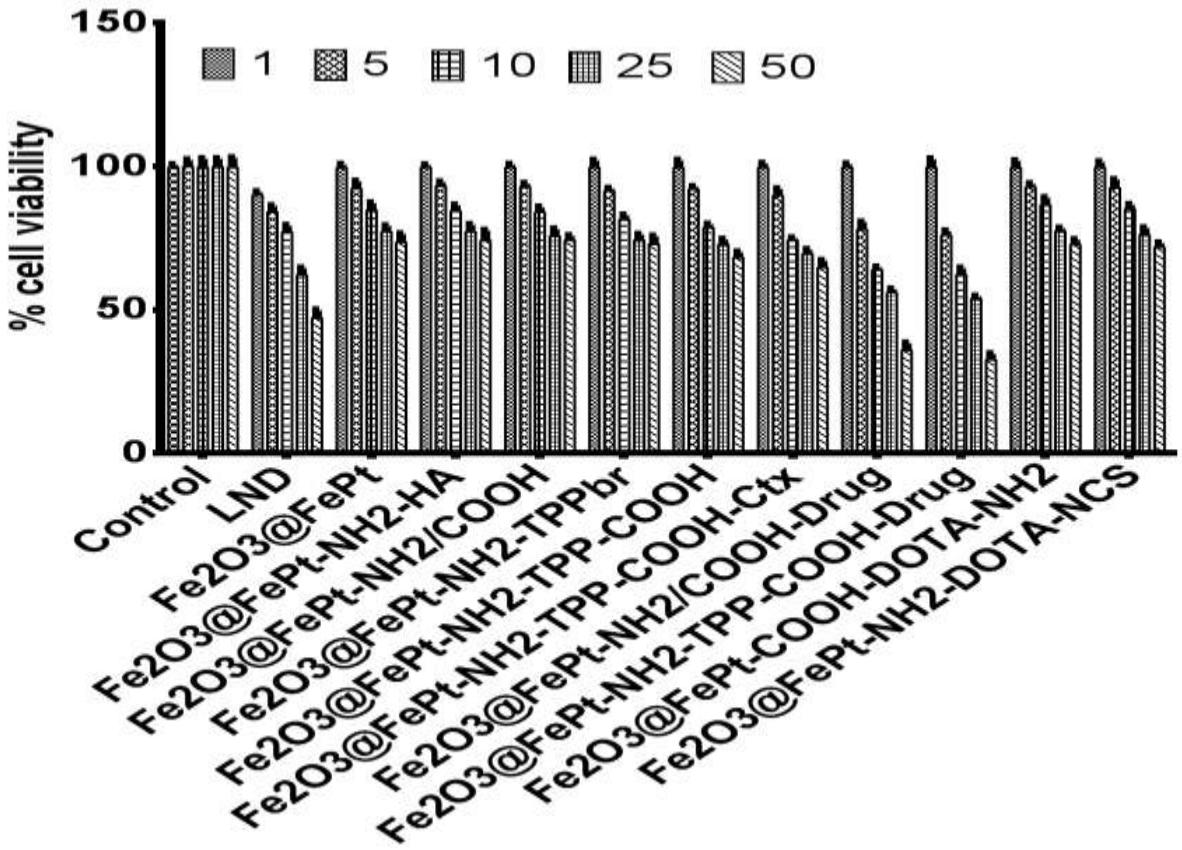

Figure 7.4**:** *In vitro* cell viability study in U87MG cells using surface modified Fe2O3@FePt nanoparticles after 24 h.

7.18. *In vitro* BBB Passage/Flux Study

Transport of pure LND, FePt, Fe_2O_3@FePt and SPANs through the in vitro BBB were determined and results are shown in Figure 7.5 and 7.6.The transport ratio of SPANs were higher than pure LND through the co-culture model at all the tested time points. Apart from co-culture method, mono layer model constructed using U-373MG cells and MDCK cells were also

included in study to understand the role of tight junction of BBB in permeation of molecules. In case of monoculture, the permeation of pure LND and SPANs was more or less similar. This can be attributed to the formation of improper junctions between the cells.

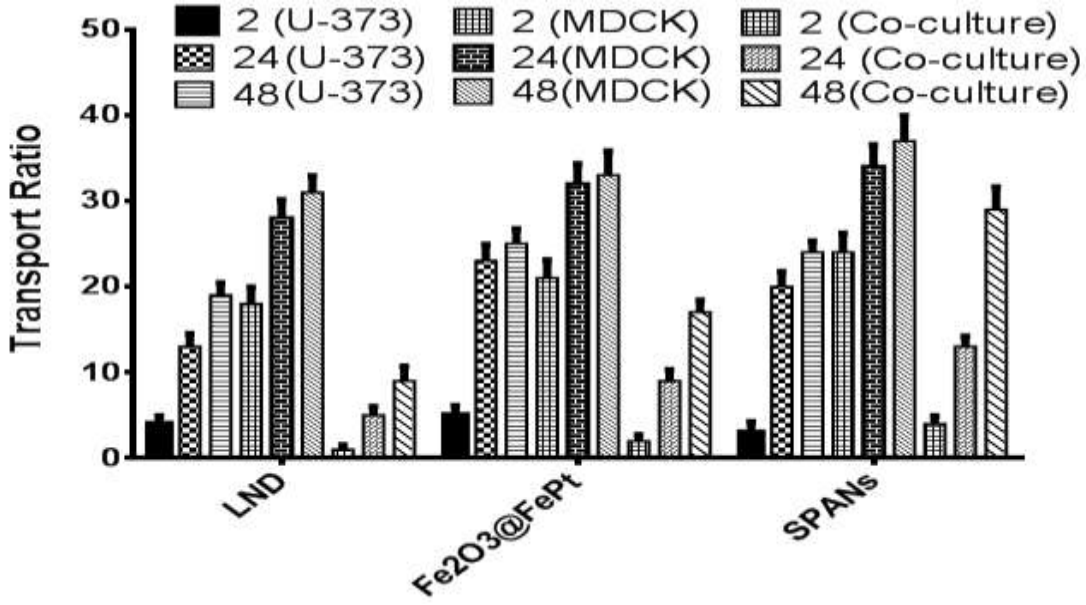

Figure 7.5**:** *In vitro* BBB passage studies for pure LND, Fe_2O_3@FePt and SPANs after 2h, 24h and 48h without AMF.

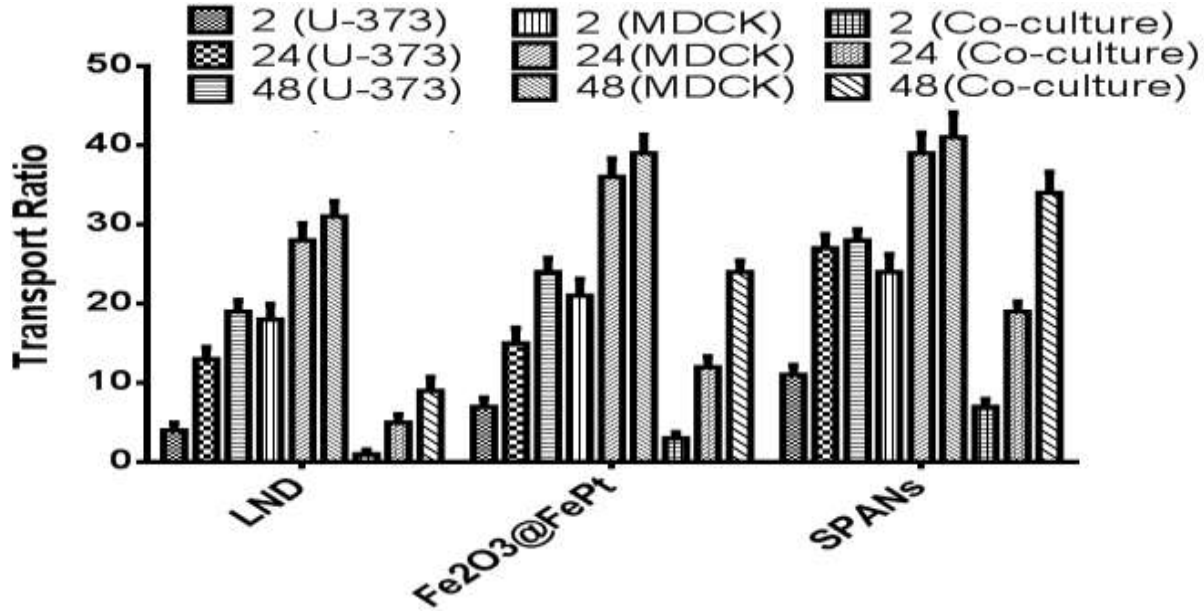

Figure 7.6**:** *In vitro* BBB passage studies for pure LND, Fe_2O_3@FePt and SPANs after 2h, 24h and 48h with AMF.

The *in vitro* BBB passage study was also performed in presence of alternating magnetic field (AMF) to assess effect of hyperthermia on permeation of nanoparticle through BBB. In the absence of magnetic field, the permeation of LND, Fe_2O_3@FePt and SPANs was time and concentration dependent while in presence of magnetic field, enhancement in transport ratio was observed even at lower time interval. The result for transport of nanoparticles in presence of AMF is shown in figure 7.7.

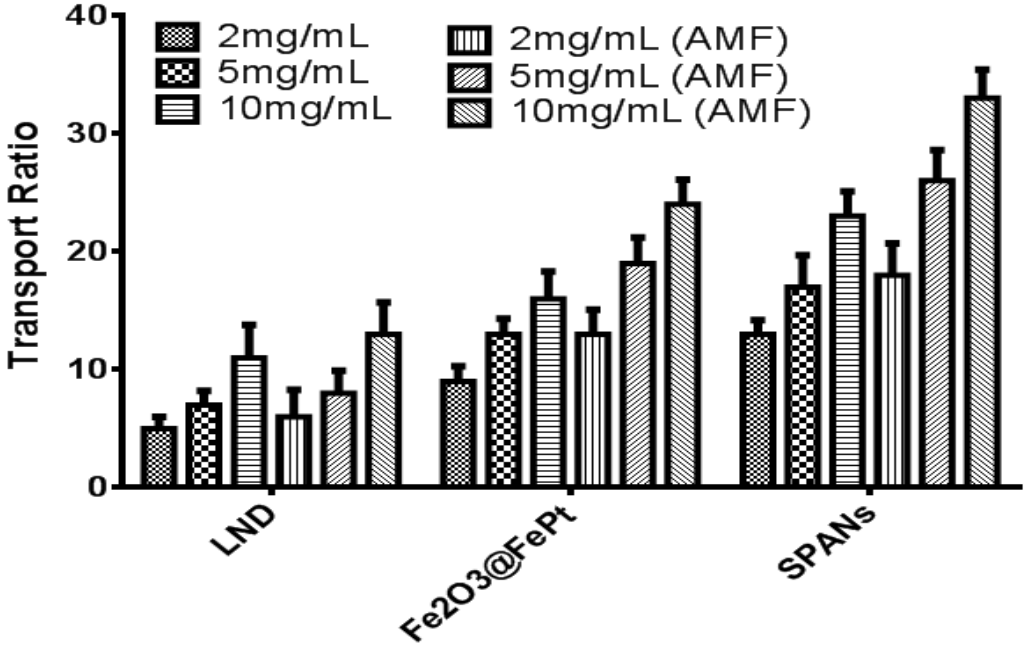

Figure 7.7: *In vitro* BBB passage studies for pure LND, Fe_2O_3@FePt and SPANs after 24h with AMF at concentration of 2mg/mL, 5mg/mL and 10mg/mL

The enhancement in transport ratio can be attributed to disruption of tight junction due to hyperthermia. This leads to increased permeation of nanoparticles inside BBB [17]. To confirm if the permeation of nanoparticles after AMF was due to cell death or BBB disruption, trypan blue exclusion test was performed. The exclusion test did not reveal cell death in any experiments after cell exposure to AMF.

7.19. Estimation of ROS Generation

ROS generation was estimated using 2′,7′-dichlorodihydrofluorescein diacetate (DCFH-DA) reaction in U87MG cells. The decomposition of H_2O_2 catalyzed by Fe generates reactive oxygen species which oxidizes various organic molecules including membrane lipids, DNA, and

proteins in cells [17]. Following cellular uptake, two ester groups in DCFHDA are hydrolyzed to hydroxyl groups in the presence of intracellular esterase. When U87MG cells are incubated with DCFHDA and SPANs, DCFH is deprotonated and converted to quinone-like DCF due to ROS generated by SPANs that fluoresces at 480 nm excitation (Figure 7.8).

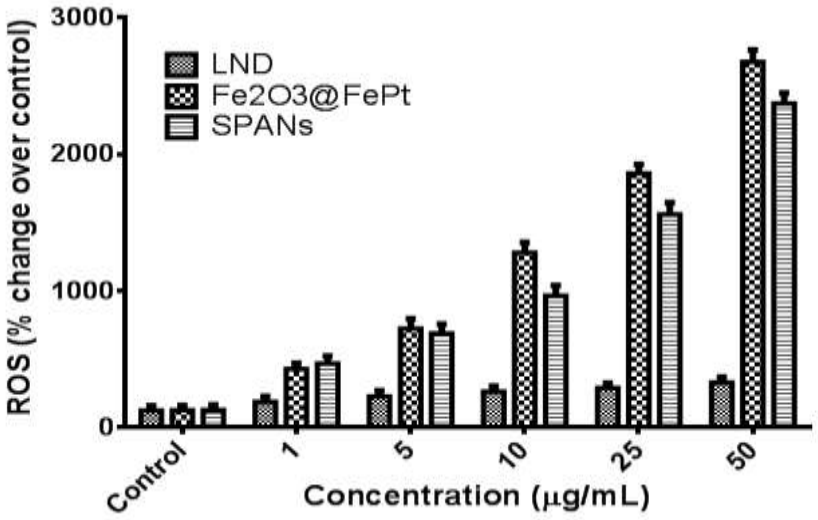

Figure 7.8: Quantitative estimation of surface ROS generation by LND, Fe_2O_3@FePt and SPANs in U87MG cells.

An increase in ROS generation was obtained with increase in concentration of SPANs which may be attributed to the fact that increase in SPANs concentration enhances Fe released after particular time interval leading to increase in ROS generation. The results further demonstrated that increase in SPANs will cause decrease in cell viability. Apart from intracellular ROS generation, surface generation of ROS by SPANs in presence of magnetic field was studied using methylene blue degradation assay (Figure 7.9). The surfaces of iron based alloy nanoparticles are capable of catalytically generating ROS through the Fenton and Haber-Weiss reactions [18]. The reaction works on the principle that SPANs reacts with H_2O_2 to generate highly reactive hydroxyl and superoxide radicals which attack and breaks bonds on methylene blue turning the molecule into colorless intermediates. By measuring methylene blue colorimetrically, the amount of degradation can be determined. Figure 7.9 represents the degradation of methylene blue in presence of magnetic field at different time periods. The result obtained from methylene blue degradation assay confirms that the presence of AMF will

enhance the net ROS generated by SPANs which would ultimately cause enhanced suppression of cell viability.

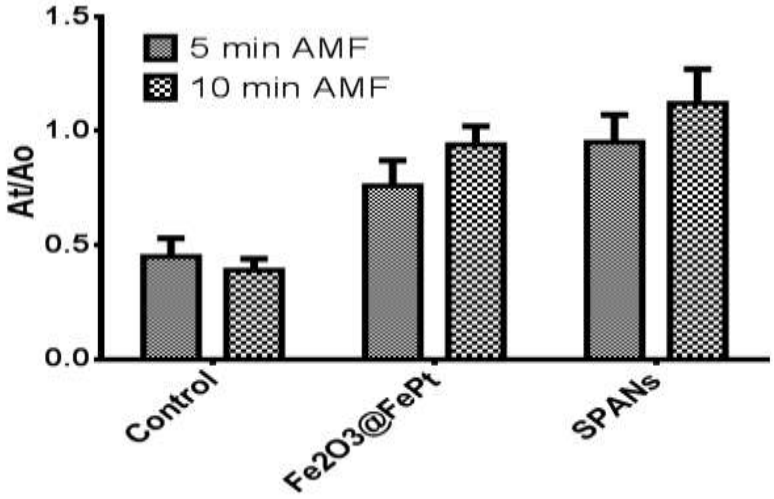

Figure 7.9: Quantitative estimation of ROS generation in U87MG cells at different concentration of Fe_2O_3@FePt and SPANs at 25µg/mL with AMF exposure for 5 and 10 minutes respectively.

In case of Fe_2O_3@FePt, the ROS generation increased with concentration and was more than that produced by SPANs. This can be attributed to the fact that SPANs had conjugated HA which makes SPANs more biocompatible than Fe_2O_3@FePt leading to decrease in ROS generation by SPANs.

7.20. Colony forming assay

Colonogenic assay was carried out to assess the long term cytotoxicity of different formulations. 600 cells (U87MG) were seeded in a 35 mm plate and after stabilization treated with SPANs and Fe_2O_3@FePt. These were removed after an incubation period of 24 h, and the plates were washed with PBS to remove traces of the drug. Cells were later incubated in complete media for a period of 8–10 days. Cells were fixed using 70% chilled methanol followed by staining using 1% Crystal violet (Figure 7.10A). Colonies were counted and the results were plotted as number of colonies versus type of nanoparticles (Figure 7.10B). The numbers of colonies for untreated, FePt treated, Fe_2O_3@FePt treated ad SPANs treated cells were found to be 295.00± 20.5, 189 ± 55, 103±44 and 45±17.5 at concentrations of 25 µg/mL respectively (P<0.05). Cancer cells show a self sufficiency towards growth signals. These results indicate that the cells lost the ability to replicate in the presence of nanoparticles.

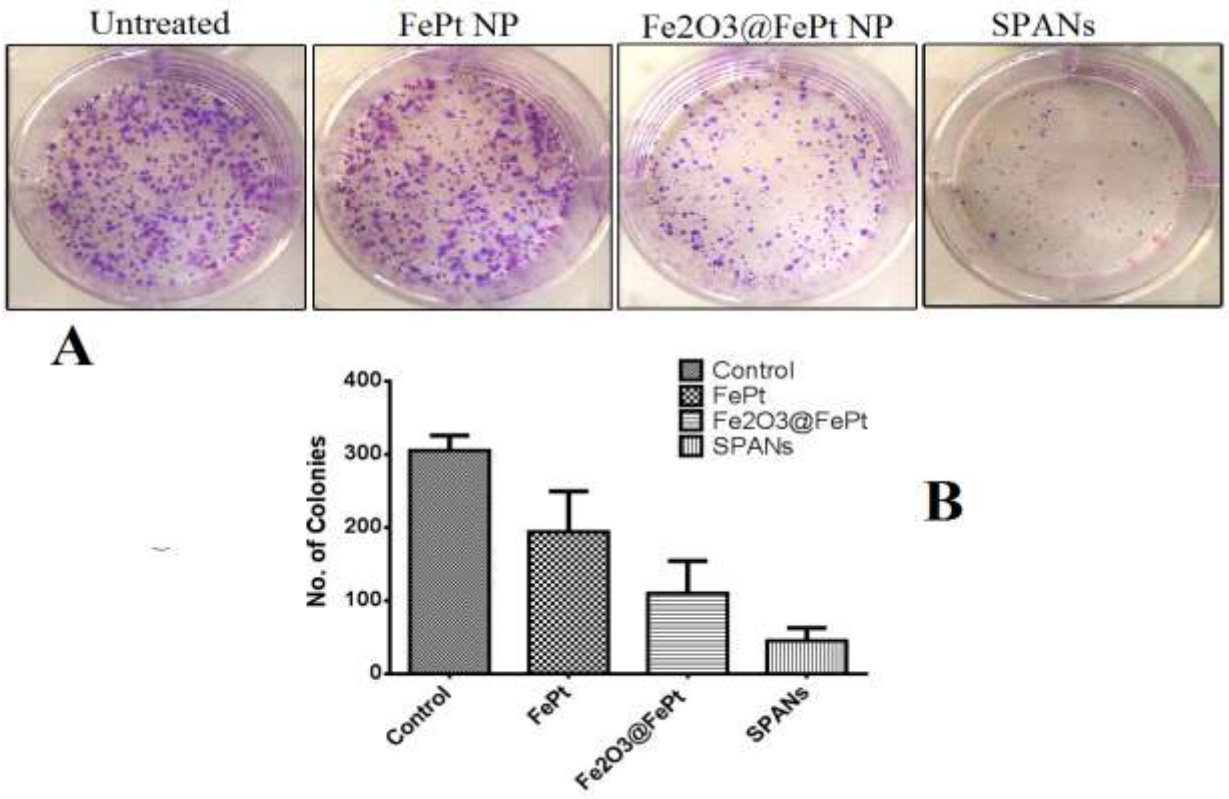

Figure 7.10: Colony forming assay of FePt nanoparticles, Fe2O3@FePt nanoparticles and SPANs qualitative (A); quantitative (B).

7.21. Estimation of Intracellular uptake

The surface charge of nanoparticles affects their cellular internalization. It has been demonstrated that nanoparticles having positive surface charge show higher degree of internalization compared to neutral or negatively charged nanoparticles owing to effective attachment to negatively charged cell membrane surface. The cellular internalization of SPANs was observed by bright field microscopy (figure 7.11A-D). The qualitative and quantitative studies on cellular internalization of SPANs in U87MG cancer cells were performed by Prussian blue staining and ferrozine based assay respectively. Figure 7.11 shows cells incubated with SPANs for different time periods (12, 24 and 48 h) by Prussian blue staining. The increase in cellular internalization of SPANs can be visualized as increase in blue cytoplasmic granular stain. The increase in cellular internalization was higher after 24 h in comparison to 12 h although visually the increase was not very high. After 48 h, the internalized SPANs were much

higher than internalization observed after 12 and 24 h. The results observed after Prussian blue stating were confirmed by colorimetric ferrozine based assay. The intracellular iron content after 12, 24 and 48 h was 8.6±1.1, 19.2±2.7 and 26.8±3.3 pg cell^{-1} respectively. The prolonged incubation time enables to reach higher intracellular loading of SPANs which is required for suppressing U87MG cell viability in a dose dependent and time dependent manner.

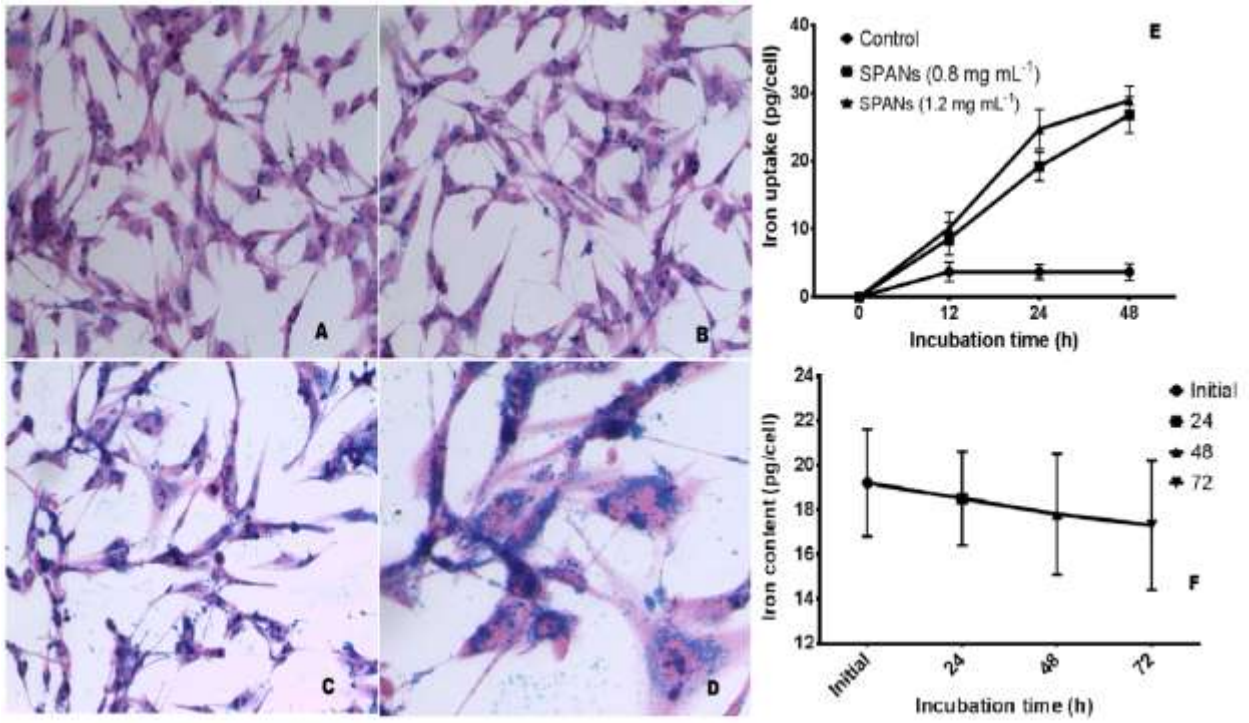

Figure 7.11: Cellular internalization of SPANs as visualized using Prussian blue staining after 12 (A), 24 (B) and 48 h (C) along with nuclear localization of SPANs after 48h (D). The quantitative estimation of SPANs in U87MG cells was done at two different dosing concentrations of 0.8mg/mL and 1.2mg/mL after 12, 24 and 48 h respectively (E), presence of SPANs inside cells was also analyzed till 72 h (F).

The intracellular uptake of SPANs was also dependent on concentration of SPANs during incubation. At incubation concentration of 0.8 mg mL^{-1}, the intracellular iron content was found to be 19.2 pg cell^{-1} after 24 h, whereas at SPANs concentration of 1.2 mg mL^{-1}, the intracellular iron content after 24 h was found to be 24.7pg cell^{-1}. From the figure 7.11, we can observe that with increase in incubation time, large aggregates of SPANs accumulated close to the nuclei and few cells even showed localization of SPANs inside nucleus. This event can be beneficial in

present case where the loaded drug i.e. LND. LND has been hypothesized to decrease the expression of angiogenic factor VEGF and Interleukin-6. It alters VEGF levels, inhibits phosphorylation of Akt and Gab 1 protein [11]. Phosphorylated Akt is responsible for angiogenesis and tumorogenesis. So, presence of LND inside nucleus will enhance the antitumor efficacy of SPANs by suppressing angiogenesis and other chain reaction initiating inside nucleus. To further analyze the persistence of SPANs inside cells, cell culture after 24 h incubation with SPANs were kept for incubation up to 72 h and samples of cell were taken and analyzed after 24, 48 and 72 h using ferrozine iron assay (figure 7.11E, 7.11F). The results suggest that although the cells keep dividing, no massive release of SPANs from cells was observed which shows that SPANs remains inside the cells for a long time.

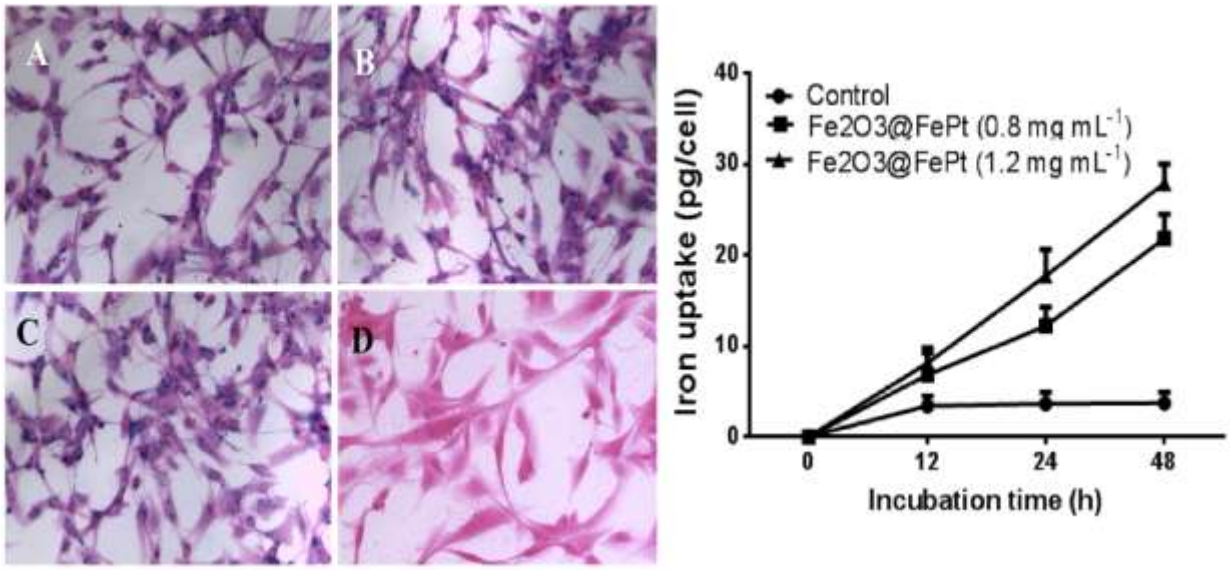

Figure 7.12**:** Cellular internalization of Fe_2O_3@FePt as visualized using Prussian blue staining after 12 (A), 24 (B) and 48 h (C) along with control 48h (D) in U87MG cells done at two different dosing concentrations of 0.8mg/mL and 1.2mg/mL after 12, 24 and 48 h respectively.

The intracellular iron content after 12, 24 and 48 h was 7.1±1.3, 14.8±2.5 and 19.8±3.1 pg $cell^{-1}$ respectively. The prolonged incubation time enables to reach higher intracellular loading of Fe_2O_3@FePt which is required for suppressing U87MG cell viability in a dose dependent and time dependent manner. At incubation concentration of 0.8 mg mL^{-1}, the intracellular iron content was found to be 12.3±1.4pg $cell^{-1}$ after 24 h, whereas at Fe_2O_3@FePt concentration of 1.2 mg mL^{-1}, the intracellular iron content after 24 h was found to be 17.5±2.1pg $cell^{-1}$ (Figure

7.12). The overall results confirm the enhanced uptake of SPANs as compared to Fe_2O_3@FePt nanoparticle which can be attributed to presence of HA which acts a ligand for CD44 receptor mediated endocytosis of nanoparticles.

7.22. Mitochondrial Targeting

Mitochondria targeting ability was assessed for M-SPANs (Fe_2O_3@FePt-NH_2/COOH-TPP-Drug-HA-Ctx) and SPANs (Fe_2O_3@FePt-NH_2/COOH-Drug-HA-Ctx). As reported earlier, lenalidomide has been shown to trigger both the extrinsic (caspase-8-dependent) and intrinsic (mitochondrial) pathways of apoptosis [11]. At least in part, this reflects the capacity of lenalidomide to antagonize pro-survival signals transduced by NFκB, resulting in the down regulation of anti-apoptotic factors such as CASP8 and FADD-like apoptosis regulator (CFLAR) and baculoviral IAP repeat containing 3 (BIRC3). Hence, accumulation of M-SPANs will lead to enhanced efficacy of nanoparticles against brain tumor. The mitochondria targeting ability of M-SPANs was assessed with respect to mitochondrial localization and disruption of mitochondrial functions as discussed below

7.22.1. Mitochondrial Localization

The study on intracellular mitochondria targeting ability of M-SPANs and SPANs was assessed in U87MG cells. Both M-SPANs and SPANs were tagged with FITC to trace their location after cellular internalization. Due to inherent fluorescent character the nanoparticles can be traced anywhere in cell. As seen from Fig. 7.12, the appearance of green fluorescence indicates the location of M-SPANs and SPANs. The MT-RFP expressing U87MG expresses mitochondrial protein corresponding to red fluorescence. Orange to yellow fluorescence in merged images indicates the co-coloration of green and red fluorescence, demonstrating the successful localization of M-SPANs-FITC in mitochondria as well as targeting ability of M-SPANs. Contrary to M-SPANs, the localization of SPANs-FITC in mitochondria was low as demonstrated by less orange to yellow fluorescence in merged images. In addition to visualization of localization, the Pearson's coefficient and overlap coefficient of the merged images in Fig. 7.12 were 0.575 and 0.284 for M-SPANs-FITC, while for FITC-SPANs (Fig. 7.13), it was 0.584 and 0.216. The higher co-localization coefficient further indicates good performance of M-SPANs in targeting mitochondria.

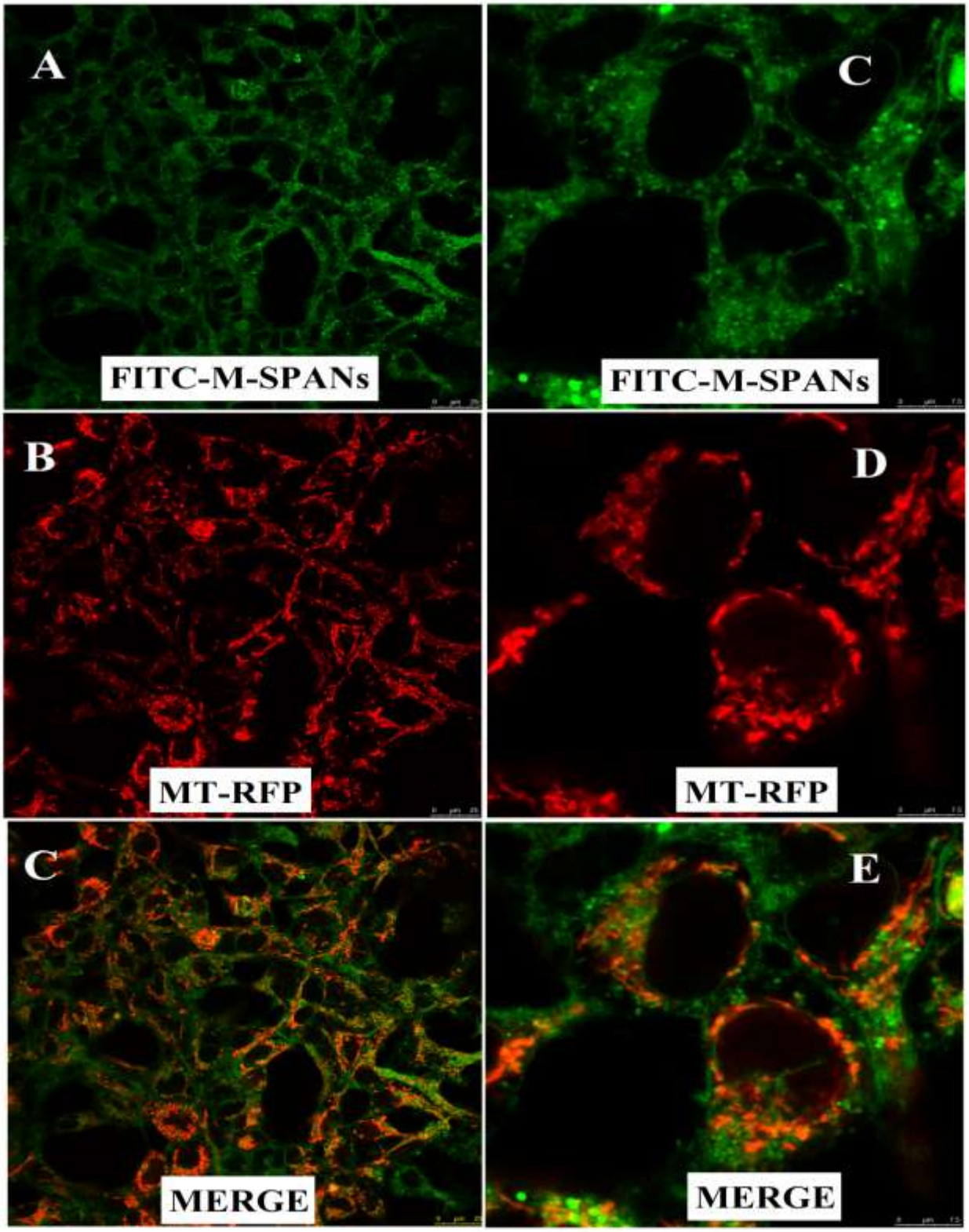

Figure 7.13**:** Confocal microscopic images of U87MG cells after being treated with FITC-M-SPANs (25µg/mL). (Mitochondria are visualized in red).

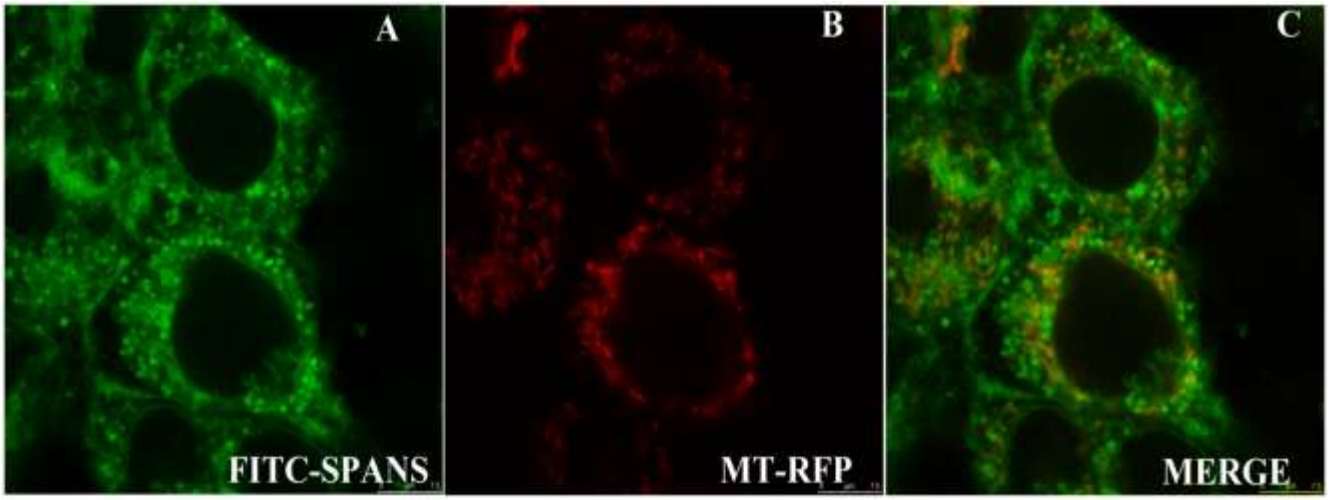

Figure 7.14: Confocal microscopic images of U87MG cells after being treated with FITC-SPANs (25µg/mL). (Mitochondria are visualized in red).

The mechanism of mitochondria targeting of M-SPANs can be understood in stepwise manner. The cationic nanoparticles are initially taken up via non specific electrostatic association and CD44 based endocytosis. The M-SPANs associate with anionic cell membrane, and then escape endosomal compartment through proton sponge effect of uncharged amines. With the assistance of lipophilic TPP groups, the cationic M-SPANs pass through the lipid bilayers of mitochondria driven by the large transmembrane potential and are finally accumulated into the mitochondrial matrix.

7.22.2. Fluorescence Analysis of Isolated Mitochondria

To further confirm the targeted accumulation of M-SPANs inside mitochondria, fluorescence analysis of isolated mitochondria was conducted based on fluorescence of FITC. Fluorescent nanoparticles without TPP conjugation (SPANs) were taken as negative control while M-SPANs were taken as positive control. Mitochondria were isolated from U87MG cells according to the isolation protocol provided by the manufacturer. The isolated mitochondria were washed twice with PBS before measurement in order to nullify fluorescent caused by free nanoparticles. As demonstrated from results shown in Figure 7.15, higher fluorescent intensity was observed in positive group i.e. M-SPANs-FITC (63.7±3.9) compared with negative group i.e. SPANs-FITC) (24.4±3.2) suggesting positive effect of mitochondria targeting TPP in facilitating mitochondrial localization. These results further confirm mitochondria targeting ability of M-SPANs.

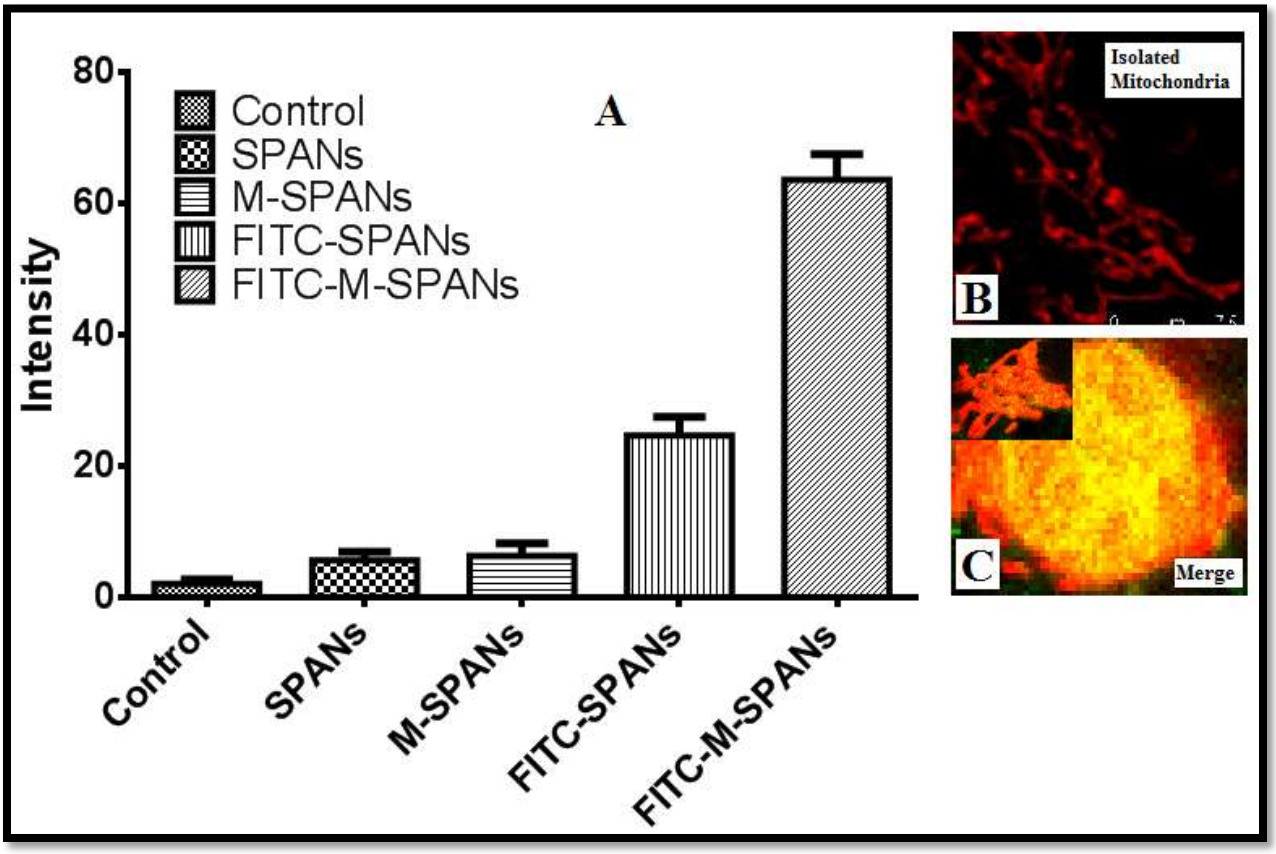

Figure 7.15: Assessment of mitochondrial targeting ability of SPANs and M-SPANs in isolated mitochondria

7.22.3. Detection of Changes in Mitochondrial Membrane Potential

Previous reports demonstrate that loss of the mitochondrial membrane potential ($\Delta\Psi m$) is an early event in mitochondria triggered apoptosis. To investigate change in mitochondrial membrane potential due to SPANs and M-SPANs, tetramethylrhodamine methyl ester (TMRE) fluorescence assay was performed in quench mode in U87MG cells keeping FCCP (carbonylcyanide 4-(trifluoromethoxy) phenylhydrazone) as positive control. TMRE stains mitochondria with active membrane potential. We can observe different levels of decrease in membrane potential when U87MG cells were treated with SPANs (194.5±7.4) and M-SPANs (147.3±17.2) (Fig. 7.16A). However, the decrease in mitochondrial membrane potential in M-SPANs was more significant than SPANs. The results suggest that mitochondria were severely damaged by M-SPANs than SPANs. Flow cytometry analysis (Fig. 7.16B) after treating U87MG cells keeping FCCP a positive control further supports above conclusion.

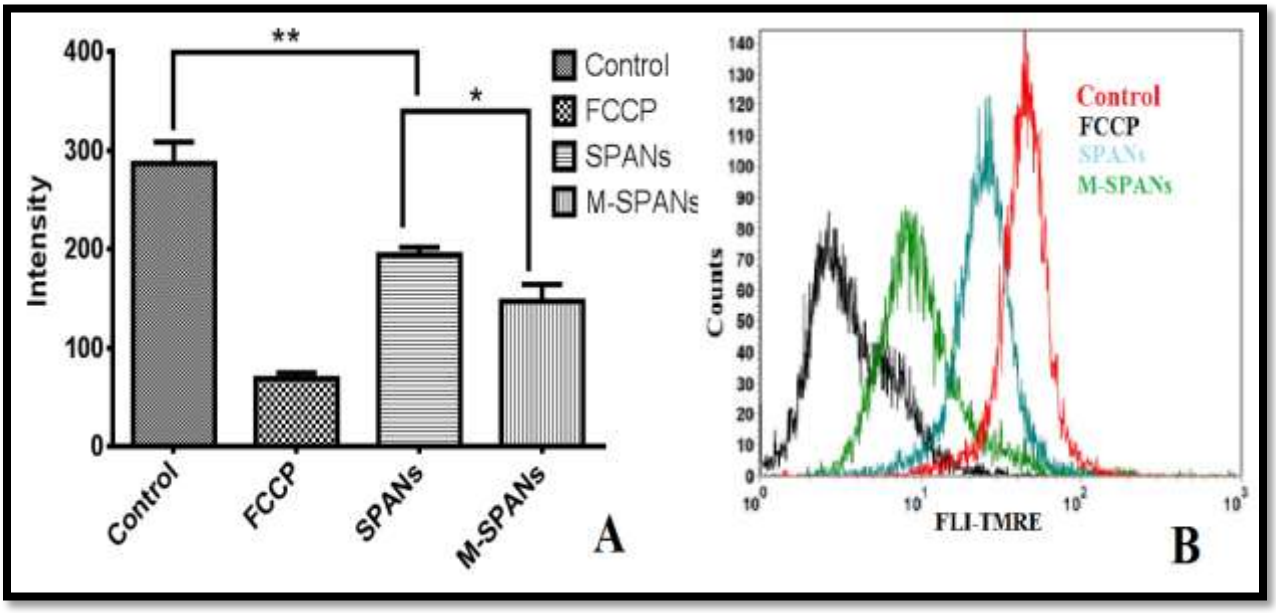

Figure 7.16**:** (A) Mitochondrial membrane potential detection after treating U87MG cells with FCCP (positive control), SPANs and M-SPANs (50µg/mL) for 24h. (B)Flow cytometry analysis after treating U87MG cells with FCCP (positive control), SPANs and M-SPANs (50µg/mL) for 24h. FLI-TMRE means fluorescence intensity of TMRE.

7.22.4. Intracellular ATP Level Detection

It has been well documented that mtDNA expression alteration are closely related to mitochondrial ATP production [19]. In order to investigate the interaction between mtDNA and nanoparticles, the detection of intracellular ATP levels was done.

Intracellular ATP levels were calculated on the basis of the standard curve. As seen from figure 7.17, decrease in mitochondrial ATP level was observed after treatment with SPANs and M-SPANs. Oligomycin was used as positive control and it shows maximum decrease in intracellular ATP level. The decrease in ATP level by SPANs (81.7±5.2) was less while with that with M-SPANs (21.2±2.9) was significant in comparison to both control and SPANs. These results confirm that the M-SPANs do affect the mitochondrial ATP production which is quite beneficial for effective tumor suppression.

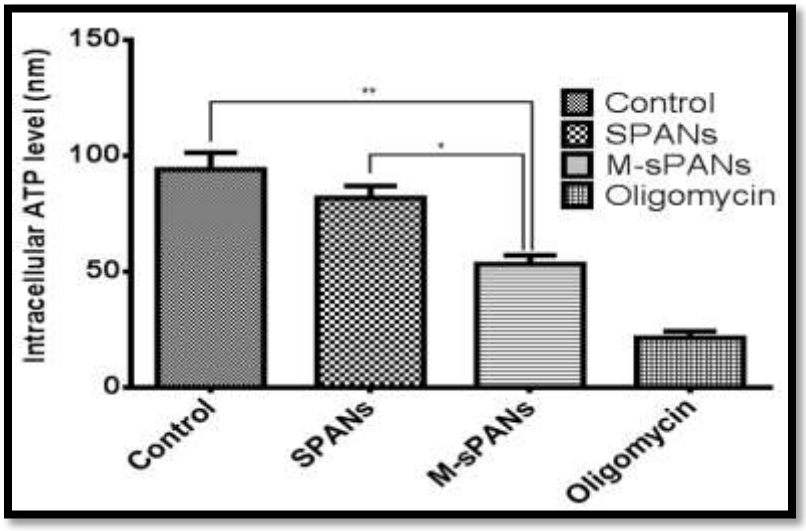

Figure 7.17: Cellular ATP level of U87MG cells after being treated with SPANs and M-SPANs for 24h at concentration of 25µg/mL Oligomycin acts as positive control.

7.22.5. Analysis of Respiratory Chain Enzymatic activity

Effect of SPANs and M-SPANs on enzymatic activity of individual mitochondrial respiratory chain complexes was measured in U87MG cells.

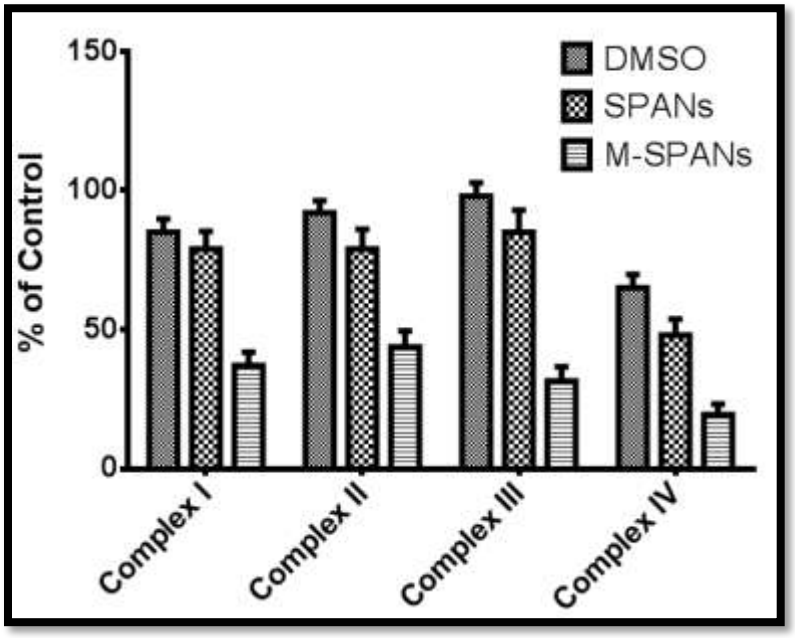

Figure 7.18**:** Activity of mitochondrial respiratory chain complexes in U87MG cells in presence of SPANs and M-SPANs.

Fig. 7.18 shows a significant inhibitory effect of M-SPANs on all four respiratory complexes i.e. complex I (37.1±3.9), complex II (43.8±5.7), complex III (31.6±5.1) and complex IV (19.5±3.8). Complex III (and IV appeared to be the most sensitive respiratory chain complex. SPANs inhibited the respiratory complex less significantly (79.2±6.3, 78.4±7.1, 84.1±7.9, 48.6±5.8) than M-SPANs. A plausible explanation of these observations may be correlated to incorporation of TPP molecule in the inner mitochondrial membrane. Since the respiratory complexes are known to be sensitive to their lipid environment and require phospholipid molecule for their activity, a high proportion of TPP molecule in the membrane could impair insulating property of membrane allowing protons to leak back into the matrix and the membrane structure required for functioning of the protein complexes [20].

References

1. T. L. Riss, R. A. Moravec, A. L. Niles, S. Duellman, H. A. Benink, T. J. Worzella, L. Minor, Assay Guidance Manual, Eli Lilly & Company and the National Center for Advancing Translational Sciences. 2004.
2. Q. Chen, L. Xu, C. Liang, C. Wang, R. Peng, Z. Liu, Photothermal therapy with immune-adjuvant nanoparticles together with checkpoint blockade for effective cancer immunotherapy. Nature Communications. 2016, 7, 1-13.
3. S. J. Chadwick, D. Salah, P. M. Livesey, M. Brust, M. Volk, Singlet Oxygen Generation by Laser Irradiation of Gold Nanoparticles. Journal of Physical Chemistry C. 2016, 120, 10647–10657.
4. Y. He, Y. Yao, S. E. Tsirka, Y. Cao, Cell-Culture Models of the Blood–Brain Barrier, DOI: 10.1161/STROKEAHA.114.005427.
5. A. Molla, M. Sahu, S. Hussain, Under dark and visible light: fast degradation of methylene blue in the presence of Ag–In–Ni–S nanocomposites, Journal of Material Chemistry A, 2015, 3, 15616-15625
6. N. A. Franken, H. M. Rodermond, J. Stap, J. Haveman, C. van Bree, Clonogenic assay of cells in vitro. Nature Protocol. 2006, 1, 2315-2319.
7. D. A. Kuhn, D. Vanhecke, B. Michen, F. Blank, P. Gehr, A. Petri-Fink, B. Rothen-Rutishauser, Different endocytotic uptake mechanisms for nanoparticles in epithelial cells and macrophages. Beilstein Journal of Nanotechnology. 2014, 5, 1625–1636.
8. J. Riemer, H. H. Hoepken, H. Czerwinska, S. R. Robinson, R. Dringen, Colorimetric ferrozine-based assay for the quantitation of iron in cultured cells. Analytical Biochemistry. 2004, 331, 370-375.
9. C. Frezza, S. Cipolat, L. Scorrano, Organelle isolation: functional mitochondria from mouse liver, muscle and cultured filroblasts. Nature Protocols. 2007, 2, 287 – 295.
10. M. Spinazzi, A. Casarin, V. Pertegato, L. Salviati, C. Angelini, Assessment of mitochondrial respiratory chain enzymatic activities on tissues and cultured cells. Nature Protocol. 2012, 7, 1235-1246.

11. V. Kotla, S. Goel, S. Nischal, C. Heuck, K. Vivek, B.Das, A. Verma, Mechanism of action of lenalidomide in hematological malignancies. Journal of Hematology and Oncology. 2009, 2, 36-46.
12. K. M. Deo, B. J. Pages, D. L. Ang, C. P. Gordon, J. R. Aldrich-Wright, Transition Metal Intercalators as Anticancer Agents—Recent Advances. International Journal of Molecular Science. 2016, 17, 1818-1837.
13. A. A. Smirnov, A. Pikulin, N. Sapogova, N. Bityurin, Femtosecond Laser Irradiation of Plasmonic Nanoparticles in Polymer Matrix: Implications for Photothermal and Photochemical Material Alteration. Micromachines. 2014, 5, 1202-1218.
14. S. Tong, C.r A. Quinto, L. Zhang, P. Mohindra, G. Bao, Size-Dependent Heating of Magnetic Iron Oxide Nanoparticles. ACS Nano, 2017, 11, 6808–6816.
15. C. L. Chen, L. R. Kuo, S. Y. Lee, Y. K. Hwu, S. W. Chou, C. C. Chen, F. H. Chang, K. H. Lin, D. H. Tsai, Y. Y. Chen, Photothermal cancer therapy via femtosecond-laser-excited FePt nanoparticles, Biomaterials. 2013, 34, 1128-1134.
16. E. C. Leuthardt, C. Duan C, M. J. Kim, J. L. Campian, A. H. Kim, M. M. Miller-Thomas, J. S. Shimony, D. D. Tran, Hyperthermic Laser Ablation of Recurrent Glioblastoma Leads to Temporary Disruption of the Peritumoral Blood Brain Barrier, PLOS One. 2016, 11, e0148613, 1-16.
17. J. Cadet, J. R. Wagner, DNA Base Damage by Reactive Oxygen Species, Oxidizing Agents, and UV Radiation, Cold Spring Harbor Perspectives in Biology. 2013, 5, a012559, 1-18.
18. C. Thomas, M. M. Mackey, A. A. Diaz, D. P. Cox. Hydroxyl radical is produced via the Fenton reaction in sub-mitochondrial particles under oxidative stress: implications for diseases associated with iron accumulation. Redox Report. 2009, 14(3), 102-108
19. J. S. Carew, P. Huang, Mitochondrial defects in cancer. Molecular Cancer. 2002, 1, 9, 1-16.
20. J. Trnka, M. Elkalaf, M. Anděl, Lipophilic Triphenylphosphonium Cations Inhibit Mitochondrial Electron Transport Chain and Induce Mitochondrial Proton Leak, PLoS One. 2015; 10(4): e0121837, 1-14.